


Millistructured Reactor as Tool for Investigating the Kinetics of Maleic Anhydride Synthesis

Mauritio Müller¹, Kira Junge¹, Gerhard Mestl², and Thomas Turek^{1,*}

DOI: 10.1002/cite.201900131

 This is an open access article under the terms of the Creative Commons Attribution-NonCommercial-NoDerivs License, which permits use and distribution in any medium, provided the original work is properly cited, the use is non-commercial and no modifications or adaptations are made.

A nearly isothermal millistructured fixed-bed reactor was used to investigate the kinetics of the selective oxidation of *n*-butane to maleic anhydride. In addition to the investigation of a broad range of industrially relevant conditions, the focus was on the influence of the reaction products on the kinetics. For this purpose, a saturator for the accurate dosing of the target product MA was developed. The experimental data were used to derive a reaction network comprising the by-products acetic and acrylic acid. Additionally, the inhibition of the associated reactions by reactants and products was investigated.

Keywords: *n*-Butane, Kinetics, Maleic anhydride, Millistructured reactors

Received: September 06, 2019; *revised:* November 25, 2019; *accepted:* December 02, 2019

1 Introduction

Maleic anhydride (MA), used for the synthesis of unsaturated polyester resins, copolymers, lubricants, etc., is one of the most important intermediate products obtained by selective oxidation [1]. Whereas in former times benzene was used as feedstock, today the selective oxidation of *n*-butane over vanadium phosphorus oxide (VPO) catalysts is established [2]. Industrially, mainly salt bath-cooled multitubular fixed-bed reactors are used for this highly exothermic process. Typically, these reactors are operated at temperatures between 390 and 430 °C and 1 to 2 bar(g) pressure at the reactor head [3]. Due to limited heat removal, hot-spots of up to 70 K occur. To avoid thermal runaway of the reactor, the butane content in the feed is usually limited to values below 1.8 vol% butane in air [2]. The achievable molar yield of the target product MA reaches up to 65 % at butane conversions between 80 and 85 % [4]. In view of an annual production of 2.8 million tons (2015) [1], there is still considerable potential for optimization. Besides the target product MA, the most important side products are CO and CO₂, which are formed by direct oxidation of *n*-butane as well as by the consecutive oxidation of MA [5]. Additionally, acetic acid (AcA) and acrylic acid (AcrA) are formed in minor amounts [6].

A critical aspect of this process is that after several hundred hours of time on stream the conversion begins to increase and at the same time the selectivity to MA decreases [6,7]. In addition to the undesirable economic consequences, this leads to the risk of a thermal runaway of the reactor due to the increasing release of energy [8]. A frequently described reason of this phenomenon is the loss of phosphorus on catalyst surface. To overcome this catalyst aging, the patent literature [7,8] suggests the addition of an organophosphorus component to the feed in combination

with a water treatment of the catalyst. Despite intensive research and long usage of this treatment in industry, the background of this phosphorus dynamics is not fully understood [7–9]. Therefore, the aim of ongoing research is to investigate the phosphorus dynamics under well-defined conditions. The millistructured reactor used in this work, originally developed by Hofmann [10], offers optimal conditions due to its virtually isothermal behavior as it allows a separation of the influences of the hotspot from other kinetic effects.

In the first step that will be described in the present publication, the experimental setup was further developed to investigate the kinetics. For this purpose, the analytics were improved to be able to record MA and organic by-products. Furthermore, the filling of the reactor was optimized to obtain reproducible experimental results. Afterwards, a systematic study of the relationship between the reaction kinetics and the operating conditions was performed. In addition to the investigation of a broad range of industrially relevant operating conditions, the focus was on the experimental examination of the reaction kinetics under the influence of the reaction products CO, CO₂, water, and MA. The aim was to clarify the connection between the various components involved and whether the associated reactions are inhibited by the reactants or reaction products. For the

¹Mauritio Müller, Kira Junge, Prof. Dr.-Ing. Thomas Turek
turek@icvt.tu-clausthal.de

Clausthal University of Technology, Institute of Chemical and Electrochemical Process Engineering, Leibnizstraße 17, 38678 Clausthal-Zellerfeld, Germany.

²Dr. Gerhard Mestl

Clariant AG, Waldheimer Straße 15, 83052 Bruckmühl, Germany.

investigation of the oxidation of MA, a two-stage saturator was developed, which allows an accurate dosing of MA to the feed. From the results of these experiments, a reaction network was derived, which also includes the by-products AcA and AcrA.

2 Experimental Setup

The experiments were performed in a millistructured fixed-bed reactor with a catalyst bed of $44 \times 72 \times 1.65$ mm, that was derived from the concept described by Hofmann [10]. As depicted in Fig. 1a, the reactor is composed of two stainless steel (1.4571) plates sealed with an outer copper gasket and an inner graphite gasket (Frenzelit, Novaphit SSTC TA-L). To keep the reactor at a desired temperature between 360 and 450 °C, it is immersed in an electrically heated vessel, containing a molten salt mixture of $\text{NaNO}_2/\text{KNO}_3$ (45:55 wt %). To get a uniform temperature distribution, the salt is circulated by distributing nitrogen (approximately 600 mL min^{-1}) at the bottom of the vessel. To measure the axial temperature profile inside the catalytic bed, there are five thermocouples in the front plate of the reactor. The first one is arranged 2 mm after the beginning of the catalyst packing, the others follow with a distance of 13 mm each.

The rectangular channel (Fig. 1b) of the reactor was filled with three different fractions (355–450 μm , 450–630 μm , and 630–800 μm) of catalyst, which were obtained by milling an industrial ring-shaped Bi-promoted VPO catalyst provided by Clariant AG. To fix the catalyst bed inside the reactor, wired cloth frits (Haver & Boecker, aperture width 0.25 mm) were used. To achieve an even distribution of the gas, the free space in front of the catalytic bed was filled with inert silicon carbide particles of the same particle size as the catalyst bed.

Fig. 2 shows a simplified schematic flow diagram of the fully automated experimental setup. As illustrated, the setup

is supplied with four different gases using mass flow controllers (MFCs) (Bronkhorst). Three MFCs are used to adjust different *n*-butane/oxygen/nitrogen mixtures at varying space velocities (up to $4800 \text{ m}_N^3 \text{ m}^{-3} \text{ h}^{-1}$). To get a uniform *n*-butane flow, the butane cylinder is heated to 45 °C and the butane lines as well as the butane MFC are heated to 60 °C to prevent condensation. The fourth MFC provides the ability to add the products CO and CO_2 to the feed stream. Water is added using an HPLC pump (Fink Carino 09 DK-PF-10-150) and a low pulsation total evaporator (ICVT, University of Stuttgart [11]). After mixing the feed components with a static mixer, the feed gases enter the aforementioned reactor, whereby all feed lines are heated to a temperature above 160 °C. To preheat the feed to salt bath temperature, the feed line is routed through the salt bath before entering the reactor. After passing through the reactor, the product gas is conducted through heated pipes (220 °C) to the product gas purification consisting of four stripping vessels. The first one is filled with stainless steel wool and serves to desublimite the formed MA, the second one is empty and holds up entrained MA particles. The last two separators are filled with deionized water and are used to wash out water-soluble by-products such as AcA and AcrA. Water and other condensable components are then removed through a process gas cooler set to a dew point of 2 °C.

After this product gas purification, the fractions of CO , CO_2 , and *n*-butane are measured with an infrared process gas analyzer (Emerson X-Stream XE) also containing a paramagnetic cell to measure the oxygen content. Additionally, the concentrations of MA, *n*-butane, and the side products AcA and AcrA before the product gas purification are measured using a gas chromatograph (Agilent 7820A) with a 30-m Agilent DB-1701 column and a flame ionization detector.

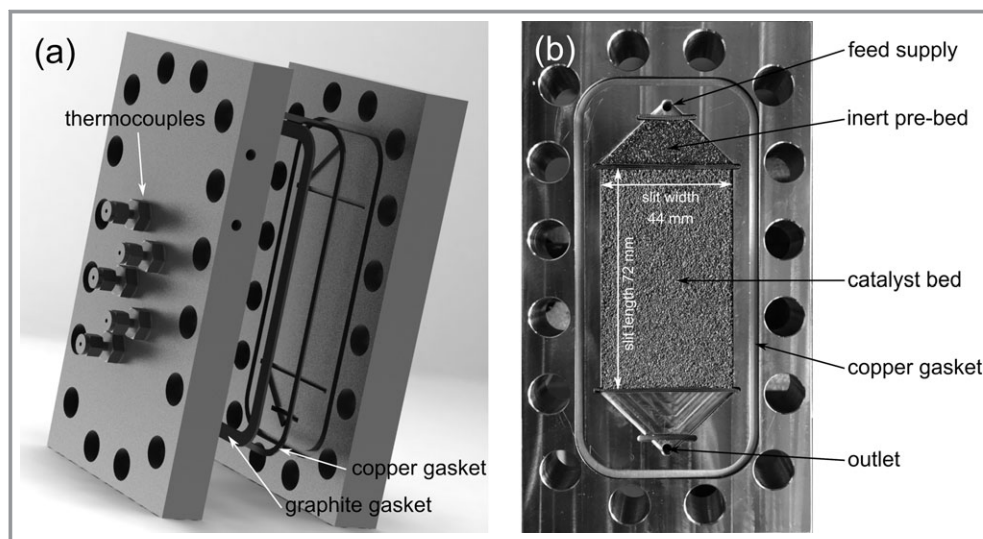


Figure 1. a) Scheme of the reactor, b) reactor filled with milled VPO catalyst.

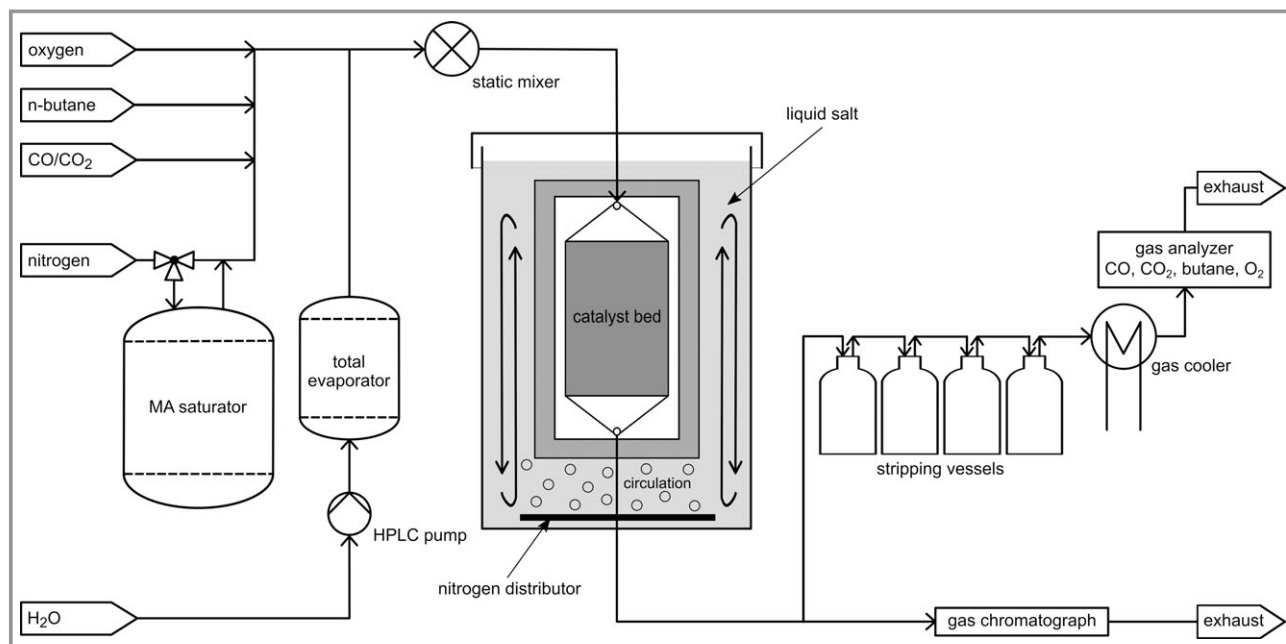


Figure 2. Schematic flow diagram of the experimental setup.

2.1 Maleic Anhydride Dosing

The addition of the product maleic anhydride, a solid at room temperature, to the feed of the reactor was realized with the aid of a two-stage saturator. This saturator depicted in Fig. 3 was developed based on the concept described by

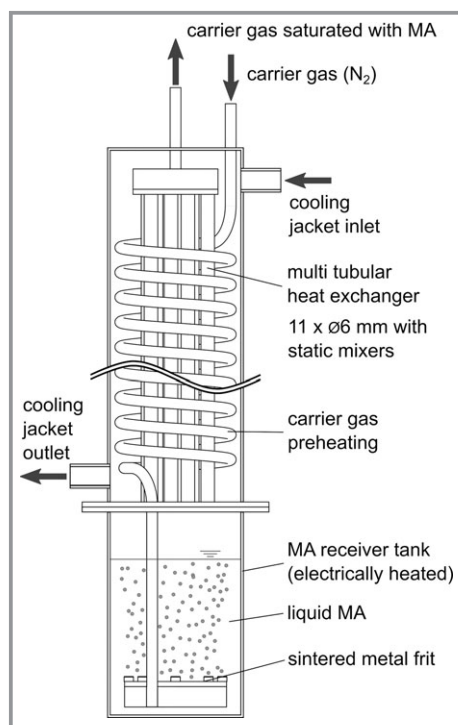


Figure 3. Schematic of the MA saturator.

Uihlein [12]. Inside the saturator, the nitrogen part of the feed stream, which is used as carrier gas, is enriched with the desired content of MA. The other components, *n*-butane and oxygen, are added after the saturator to prevent oxidation of MA or dissolution of *n*-butane in MA inside the saturator.

To preheat the nitrogen stream, it is passed through a spiral tube in the heat exchanger of the second (upper) part of the saturator. In the first stage, the preheated nitrogen stream is distributed through a sintered stainless steel frit (pore size 14 μm) into liquid MA at 110 °C. Subsequently in the second part, the MA content is adjusted to the desired value by condensing out excess MA by cooling down (60 to 85 °C) the saturated gas stream in a multitubular heat exchanger tempered with a circulation thermostat.

Special emphasis is paid to the heat exchanger within the second part of the saturator. In a first version, it consisted of simple tubes without built-in components. Experiments showed, however, a strong dependence of the MA content at the output of the saturator on the filling level and especially the temperature of the receiver tank. Theoretically, the MA content depends only on the temperature in the heat exchanger and should be independent of the nitrogen flow rate as well as the temperature and level of the storage tank. However, the lower the temperature or filling level was, the higher was the MA content at the output. A possible reason for this behavior, which contradicts the vapor pressure curve, was a lack of condensation of excess MA in the heat exchanger. The higher the temperature and, therefore, the vapor pressure of MA before cooling down, the higher is the oversaturation inside the heat exchanger. Since a homogeneous condensation requires a certain degree of

supersaturation [13], it is possible that at low temperatures not enough condensation nuclei are formed which allow a complete condensing out of excess MA. As such oversaturation is not required for heterogeneous condensation on surfaces [13] and the required oversaturation for homogeneous condensation decreases with increasing fluid velocity and turbulence [14], static mixers were introduced into the tubes of the heat exchanger. The resulting improved condensation and better heat exchange made it possible to achieve an MA content that was independent of volume flow, temperature, and filling level of the receiver tank. This improved two-stage design allows a very accurate dosing of MA, the observed deviations from the few available data in the literature [15] are below 8%. The reproducibility of the dosing of MA is quite good, the deviations are less than 2%.

3 Experimental Procedure

To investigate the kinetics, a series of experiments using the aforementioned setup was conducted. Before the actual experiments could be started, the filling of the reactor had to be investigated in more detail. In former experiments, despite identical catalyst masses, large differences in the performance of the reactor could be observed, which were also apparent in the measured pressure drop. The reason of this lack of reproducibility of experiments could be attributed to the filling of the slit reactor. Therefore, the following filling procedure was developed.

In the first step, 5.55 g of crushed catalyst material is supplied through the feed line of the reactor. Then, the catalyst bed is compacted under shaking the whole reactor with a vibrating sieve tower for 2 min. After the installation of the frit on the top of the catalyst bed and filling in the inert pre-bed, the catalyst bed is compacted by vibrating it again for 4 min. This subsequent compaction reduces channeling effects, resulting in significantly lower deviations in pressure drop and conversion between different experiments. Without this treatment, differences in pressure drop and conversion of up to 15 and 10% could be observed between the experiments, whereas these are smaller than 2 and 3% after compaction.

Each experiment took between 800 and 1500 h and was executed according to the following procedure:

- (1) The catalyst-filled reactor was immersed under nitrogen flow (300 mL min^{-1}) into the salt bath at approximately 320°C . After switching on the salt bath circulation, the temperature of the salt bath was heated up with $0.5^\circ\text{C min}^{-1}$ to 430°C . As soon as the salt temperature reached 360°C , the butane and oxygen supply were started.
- (2) After start-up, the catalyst was equilibrated at 430°C , 1.5% *n*-butane in air, 1.2 bar, and a space velocity of $4800 \text{ m}_\text{N}^3 \text{ m}^{-3} \text{ h}^{-1}$. These conditions were also chosen as a reference condition to compare the different experiments with each other and to evaluate catalyst aging.

- (3) As soon as a steady state was attained, the variation of the operating conditions according to a design of experiments (DOE) was started. Within these variations, salt bath temperatures between 380 and 440°C , butane concentrations between 1.2 and 2.1%, oxygen contents between 16 and 21%, and space velocities between 3900 and $4800 \text{ m}_\text{N}^3 \text{ m}^{-3} \text{ h}^{-1}$ were investigated. Additionally, some experiments were carried out under adding of the products water, MA, CO, and CO_2 . Each test point was maintained for 12 to 48 h, until a new steady state was reached.

The measured data are analyzed according to the following definitions of conversion X and selectivity S_i to component i . In these definitions, \dot{n}_i and $\dot{n}_{i,0}$ are the molar flow rates of the respective component i at the reactor inlet and outlet, respectively, while χ_i is the number of carbon atoms of component i .

$$X = \frac{\dot{n}_{\text{C}_4\text{H}_{10},0} - \dot{n}_{\text{C}_4\text{H}_{10}}}{\dot{n}_{\text{C}_4\text{H}_{10},0}} \quad (1)$$

$$S_i = \frac{\chi_i}{4} \frac{\dot{n}_i - \dot{n}_{i,0}}{\dot{n}_{\text{C}_4\text{H}_{10},0} - \dot{n}_{\text{C}_4\text{H}_{10}}} \quad (2)$$

4 Results and Discussion

During startup of the experiments, it was observed that in the first 10 days there was a continuous decrease in catalyst activity with a simultaneous increase in selectivity to the target product MA. The duration of the equilibration phase is thus considerably longer than the 40 hours described by Lesser et al. [6] for the same catalyst but is in the same order of magnitude as stated by Schulz et al. [16]. One possible reason for Lesser's much faster equilibration period is the higher hot spot temperature, which was 450°C compared to the reactor temperature of 430°C in the current experiments. An increase in temperature would shorten the running-in period, which would have, however, the disadvantage of very high conversions. Since the conversion would rise above typical industrial values, an increase in temperature to shorten the running-in phase was avoided.

In the first experimental runs, the reactor was operated without addition of any products. By periodically repeating the reaction conditions of the equilibrating phase, it was possible to demonstrate that no significant ageing of the catalyst occurred under these conditions, even after 45 days on stream. The observed differences in conversion and selectivities were all in the range of the measurement inaccuracy and did not show an unambiguous trend. Furthermore, it could be demonstrated that a broad range of conversion between 25 and up to 93% can be achieved with the investigated operating conditions. The corresponding selectivities to the products are depicted in Fig. 4.

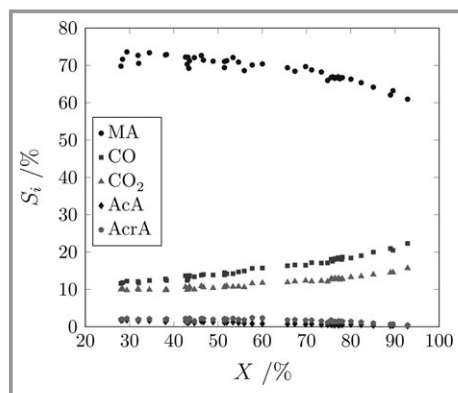


Figure 4. Selectivities S_i to MA, CO, CO₂, AcA, and AcrA as a function of the conversion X (380–440 °C, 1.2–2.1 % butane, 16–21 % O₂, 3900–4800 m_N³m⁻³h⁻¹).

To exclude the influence of mass transfer resistances on the reactor performance, experiments with three different catalyst fractions (355–450, 450–630, and 630–800 μm) were compared with each other. As no significant differences could be observed, mass transport resistances seem to play a minor role. These results are consistent with the calculated catalyst efficiency obtained by simulating the reactor with a heterogeneous reactor model, using the gPROMS software package and the kinetics of Lesser et al. [3]. The calculated catalyst efficiency, i.e., the ratio of observed to theoretical intrinsic reaction rate, is greater than 95 % for all conditions considered. Only for temperatures higher than 430 °C and the largest catalyst fraction, smaller catalyst efficiencies were calculated, which are still above 90 %. For this reason, the following results refer to the middle catalyst fraction of 450–630 μm.

As already shown by Hofmann [10] for a reactor with a slit width of 1.5 mm instead of the 1.65 mm used here, the reactor behaves almost isothermally. Even at high space velocities of up to 4800 m_N³m⁻³h⁻¹ and over 90 % conversion, the measured temperature of the catalyst bed is at maximum 5 K above the temperature of the surrounding salt bath. These low hot spots compared to industrial reactors allow an operation at higher butane concentrations than the usual maximal 1.8 % [2] in industry. As shown by Hofmann [10], a runaway of the reactor does not occur even at concentrations significantly above (up to 4.5 %) the lower explosion limit. To ensure comparability with industrial conditions, the concentration of butane was limited to 2.1 % for the present work.

To investigate the influence of the reaction conditions, a series of experiments was conducted under varying salt bath temperature, space velocity, and butane concentration. Fig. 5a shows that the

conversion increases with rising temperature. As described in the literature [5], the measured selectivity to MA decreases with increasing conversion, which is due to the growing influence of over-oxidation of MA to CO and CO₂. This is also reflected in the increasing selectivities to CO and CO₂. The influence of the butane concentration is illustrated in Fig. 5b. From the data presented, it becomes apparent that the conversion decreases with increasing butane content, which indicates a butane reaction order of less than one or an inhibition by butane. Inhibition by butane is frequently assumed in the literature and described by Buchanan and Sundaresan [17], Uihlein [12], Becker [18], Lorences et al. [19], Brandstädter [20], Lesser [9], and many other authors. The influence of the butane content on the selectivities is rather small; there is a slight increase in selectivity to MA and a slight decrease in selectivities to CO and CO₂. This shows that the oxidation of butane to CO_x must also be inhibited by butane.

In addition to CO and CO₂, AcA and AcrA were also formed as undesirable by-products. Further by-products or intermediate products could not be detected. This is in accordance with the literature [21], according to which intermediates can only be detected at high butane or low oxygen contents. AcA and AcrA are formed with selectivities of up to 3 % each, whereas their content decreases with increasing conversion. While Lorences et al. [19] also described this trend for AcA, they observed a rising selectivity to AcrA with increasing temperature and conversion. Since both fractions decrease with increasing conversion, both AcA and AcrA must be oxidized further to CO_x. In experiments involving the co-feeding of CO and CO₂, it could be demonstrated that these components have no influence on the kinetics, which is in agreement with Uihlein's [12] results. Moreover, also an oxidation of CO to CO₂ could not be observed.

The influence of water was investigated in a series of measurements by adding up to 4 % water to the feed. Within a few minutes, water leads to a decrease in conversion,

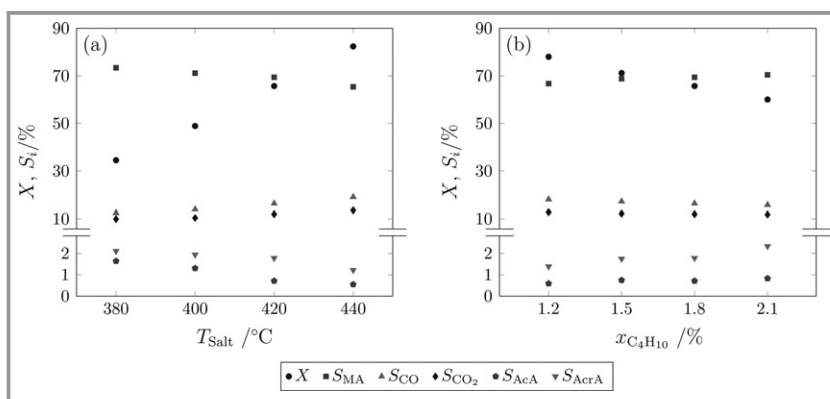


Figure 5. Conversion X and selectivities S_i as a function of a) salt bath temperature T_{Salt} (1.8 % butane, 21 % O₂, 4500 m_N³m⁻³h⁻¹) and b) butane content $x_{\text{C}_4\text{H}_{10}}$ (420 °C, 21 % O₂, 4500 m_N³m⁻³h⁻¹).

which is in accordance with the results of Arnold and Sundaresan [22], Contractor et al. [23], and Lesser [9]. After this immediate change, there was a further but much slower change in catalyst performance within the next few days, like described by Arnold and Sundaresan [22]. After switching off the water supply, the original catalyst performance was restored, so both effects seem to be reversible. Irreversible effects as described in [22] could not be observed, even after longer periods of water supply. As depicted in Fig. 6, the influence of water on the conversion rises with increasing water content. The selectivity to the target product MA does not seem to be influenced by water, which is in contrast to Arnold and Sundaresan [22], who observed an increase in selectivity. In contrast to the selectivity to MA, the selectivities to CO and CO₂ decrease with increasing water content, accompanied by a slight decrease in the CO/CO₂ ratio. On the other hand, there is a strong increase in the selectivities to the by-products AcA and AcrA, up to selectivities of more than 4 %, which indicates an inhibition of oxidation to CO and CO₂.

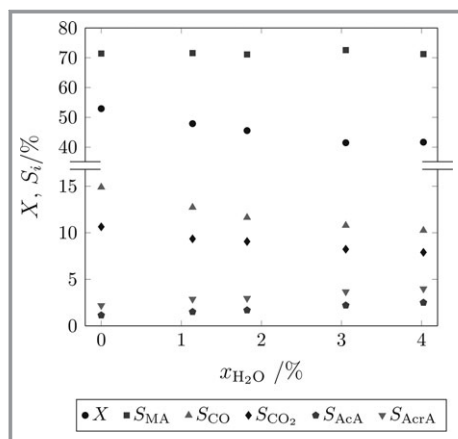


Figure 6. Conversion X and selectivities S_i as a function of the water content x_{H_2O} (1.5 % butane, 400 °C, 21 % O₂, 4500 m_N³m⁻³h⁻¹).

To investigate the consecutive oxidation of MA, some experiments were carried out under up to 1 % of MA supply. The experiments were performed both under co-dosing of butane and MA as well as without butane. It could be observed that MA has no influence on the oxidation of butane. Thus, an inhibition of butane oxidation by MA, as described in some older publications on the kinetics of *n*-butane oxidation (e.g., [24]), can be excluded. From the experiments without butane, it becomes evident that the oxidation of MA is inhibited by MA itself, since the conversion of MA decreases with increasing MA content (Fig. 7). While the addition of MA has no effect on the conversion of butane, butane seems to inhibit the oxidation of MA. This is shown by the amounts of CO and CO₂ released under co-dosing, which are smaller than the sum of the released amounts from the individual experiments in which only butane or MA was added. Similar to the oxidation of

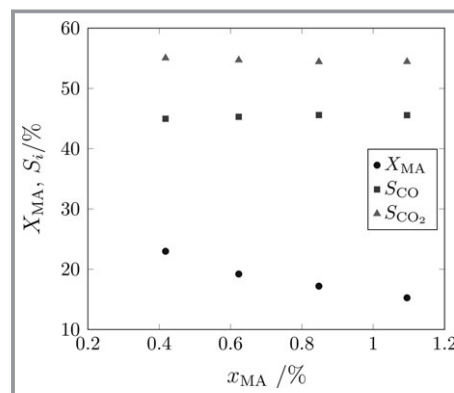


Figure 7. Conversion X_{MA} and selectivities S_i to CO and CO₂ for the oxidation of MA as a function of the MA content x_{MA} at the reactor inlet (400 °C, 21 % O₂, 4500 m_N³m⁻³h⁻¹).

butane, it was observed that the subsequent oxidation of MA is inhibited by water. In all cases, with and without water, it can be observed that the ratio of CO/CO₂ is independent of the reaction conditions and equals approximately 45:55 %. A formation of AcA and AcrA from MA could not be observed in any case.

5 Conclusion

The kinetics of selective oxidation of *n*-butane to maleic anhydride were investigated in a nearly isothermal milli-structured fixed-bed reactor filled with fine catalyst powder so that mass transport resistances can be neglected. To investigate the influence of the product MA, a saturator was developed for its precise dosage. Based on the results of experiments in a broad industrially relevant range, including the addition of products, the reaction network shown in Fig. 8 was developed, which also includes the by-products. It was shown that the oxidation of butane as well as the oxidation of MA is inhibited by water and butane itself, whereby water has no significant influence on the selectivity to MA. The effects of water were fully reversible and had no effect on

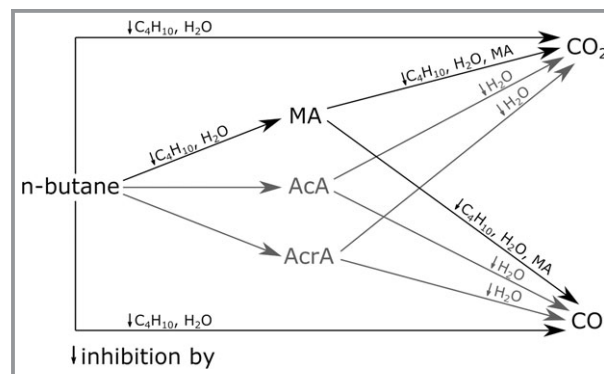


Figure 8. Reaction network with by-products. The labels above the arrows indicate an inhibition by the specified components.

the catalyst performance after switching off the water supply. Co-dosing experiments with MA have shown that there is no product inhibition of the oxidation of butane by MA, as is often described in literature. The by-products AcA and AcrA were detected in significant quantities, especially at low temperatures and conversions as well as under water supply. Therefore, both components must be oxidized to CO and CO₂, whereby the subsequent oxidation is favored by high temperatures and low water contents. The corresponding reaction network is summarized in Fig. 8 together with information on the inhibition of each individual reaction.

A possible reason for the observed inhibition of the oxidation of butane and MA by butane (and MA) could be a competitive adsorption of butane, MA, and oxygen on the catalyst surface. In a variety of publications (e.g., [9]) the process is described with an Eley-Rideal-type kinetics, whereby it is assumed that oxygen adsorbs on the catalyst surface and butane and MA react directly from the gas phase. A concurrent adsorption of butane and MA could therefore lead to a reduction of the adsorbed oxygen and, thus, inhibit the reaction. Other authors (e.g., [19]), in contrast, assume a redox mechanism according to Mars and van Krevelen [25]. The inhibition is attributed to a reduction of the active centers of the catalyst by the oxidation of butane and MA, which changes the redox behavior of the catalyst. The observed inhibition by water could be explained in both models by competing adsorption respectively by adsorption of water on the reduced catalyst surface and, therefore, the inhibition of the reoxidation of the catalyst. A precise clarification of the reason for the inhibitions is not yet possible on the basis of the currently available data but will be examined in more detail in future publications.

The authors thank Clariant AG for providing the VPO catalyst.

Symbols used

\dot{n}_i	[mol min ⁻¹]	molar flowrate of component <i>i</i> at reactor outlet
$\dot{n}_{i,0}$	[mol min ⁻¹]	molar flowrate of component <i>i</i> at reactor inlet
S_i	[-]	selectivity to component <i>i</i>
x_i	[-]	mole fraction of component <i>i</i>
X_i	[-]	conversion of component <i>i</i>
χ_i	[-]	number of carbon atoms of component <i>i</i>

Abbreviations

AcA	acetic acid
AcrA	acrylic acid

MA	maleic anhydride
VPO	vanadium phosphorus oxide

References

- [1] G. Mestl, D. Lesser, T. Turek, *Top. Catal.* **2016**, *59* (17–18), 1533–1544. DOI: <https://doi.org/10.1007/s11244-016-0673-0>
- [2] K. Lohbeck, H. Haferkorn, W. Fuhrmann, N. Fedke, *Maleic and Fumaric Acids*, in Ullmann's Encyclopedia of Industrial Chemistry, Wiley-VCH, Weinheim **2000**.
- [3] D. Lesser, G. Mestl, T. Turek, *Chem. Eng. Sci.* **2017**, *172*, 559–570. DOI: <https://doi.org/10.1016/j.ces.2017.06.049>
- [4] F. Trifirò, R. K. Greasselli, *Top. Catal.* **2014**, *57* (14–16), 1188–1195. DOI: <https://doi.org/10.1007/s11244-014-0285-5>
- [5] G. Centi, F. Trifirò, J. R. Ebner, V. M. Franchetti, *Chem. Rev.* **1988**, *88* (1), 55–80. DOI: <https://doi.org/10.1021/cr00083a003>
- [6] D. Lesser, G. Mestl, T. Turek, *Appl. Catal., A* **2016**, *510*, 1–10. DOI: <https://doi.org/10.1016/j.apcata.2015.11.002>
- [7] G. T. Click, B. J. Barone, *US Patent 4 515 899*, **1985**.
- [8] J. R. Ebner, *US Patent 5 185 455*, **1993**.
- [9] D. Lesser, *Dynamic Behavior of Industrial Fixed Bed Reactors for the Manufacture of Maleic Anhydride*, Dissertation, Technische Universität Clausthal **2016**.
- [10] S. Hofmann, T. Turek, *Chem. Eng. Technol.* **2017**, *40* (11), 2008–2015. DOI: <https://doi.org/10.1002/ceat.201700093>
- [11] A. Freund, G. Friedrich, C. Merten, G. Eigenberger, *Chem. Ing. Tech.* **2006**, *78* (5), 577–580. DOI: <https://doi.org/10.1002/cite.200500174>
- [12] K. Uihlein, *Butanoxidation an VPO-Wirbelschichtkatalysatoren*, Dissertation, Universität Karlsruhe (TH) **1993**.
- [13] J. E. McDonald, *Am. J. Phys.* **1962**, *30* (12), 870–877. DOI: <https://doi.org/10.1119/1.1941841>
- [14] L. Shmidt, J. Shmidt, *Chem. Eng. Commun.* **1984**, *30* (1–2), 83–97. DOI: <https://doi.org/10.1080/00986448408911117>
- [15] D. R. Stull, *Ind. Eng. Chem.* **1947**, *39* (4), 517–540. DOI: <https://doi.org/10.1021/ie50448a022>
- [16] C. Schulz, F. Pohl, M. Driess, R. Glaum, F. Rosowski, B. Frank, *Ind. Eng. Chem. Res.* **2019**, *58* (7), 2492–2502. DOI: <https://doi.org/10.1021/acs.iecr.8b04328>
- [17] J. S. Buchanan, S. Sundaresan, *Appl. Catal.* **1986**, *26*, 211–226. DOI: [https://doi.org/10.1016/S0166-9834\(00\)82553-1](https://doi.org/10.1016/S0166-9834(00)82553-1)
- [18] C. Becker, *Katalytische Wandreaktor-konzepte für MSA-Synthese und Methanol-Dampfreformierung*, Dissertation, Universität Stuttgart **2002**.
- [19] M. J. Lorences, G. S. Patience, F. V. Diez, J. Coca, *Ind. Eng. Chem. Res.* **2003**, *42* (26), 6730–6742. DOI: <https://doi.org/10.1021/ie0302948>
- [20] W. M. Brandstädter, *Partial Oxidation of Raffinate II and Other Mixtures of n-Butane and n-Butenes to Maleic Anhydride in a Fixed-Bed Reactor*, Dissertation, Universität Karlsruhe (TH) **2007**.
- [21] B. Chen, E. J. Munson, *J. Am. Chem. Soc.* **1999**, *121* (47), 11024–11025. DOI: <https://doi.org/10.1021/ja9929180>
- [22] E. W. Arnold, S. Sundaresan, *Appl. Catal.* **1988**, *41*, 225–239. DOI: [https://doi.org/10.1016/S0166-9834\(00\)80394-2](https://doi.org/10.1016/S0166-9834(00)80394-2)
- [23] R. M. Contractor, H. S. Horwitz, G. M. Sisler, E. Bordes, *Catal. Today* **1997**, *37* (1), 51–57. DOI: [https://doi.org/10.1016/S0920-5861\(96\)00257-X](https://doi.org/10.1016/S0920-5861(96)00257-X)
- [24] R. K. Sharma, D. L. Cresswell, E. J. Newson, *AIChE J.* **1991**, *37* (1), 39–47. DOI: <https://doi.org/10.1002/aic.690370103>
- [25] P. Mars, D. W. van Krevelen, *Chem. Eng. Sci.* **1954**, *3*, 41–59. DOI: [https://doi.org/10.1016/S0009-2509\(54\)80005-4](https://doi.org/10.1016/S0009-2509(54)80005-4)